iScience, Volume *25*

Supplemental information

Agent-based computational modeling of glioblastoma predicts that stromal density is central to oncolytic virus efficacy

Adrianne L. Jenner, Munisha Smalley, David Goldman, William F. Goins, Charles S. Cobbs, Ralph B. Puchalski, E. Antonio Chiocca, Sean Lawler, Paul Macklin, Aaron Goldman, and Morgan Craig

SUPPLEMENTARY FIGURES

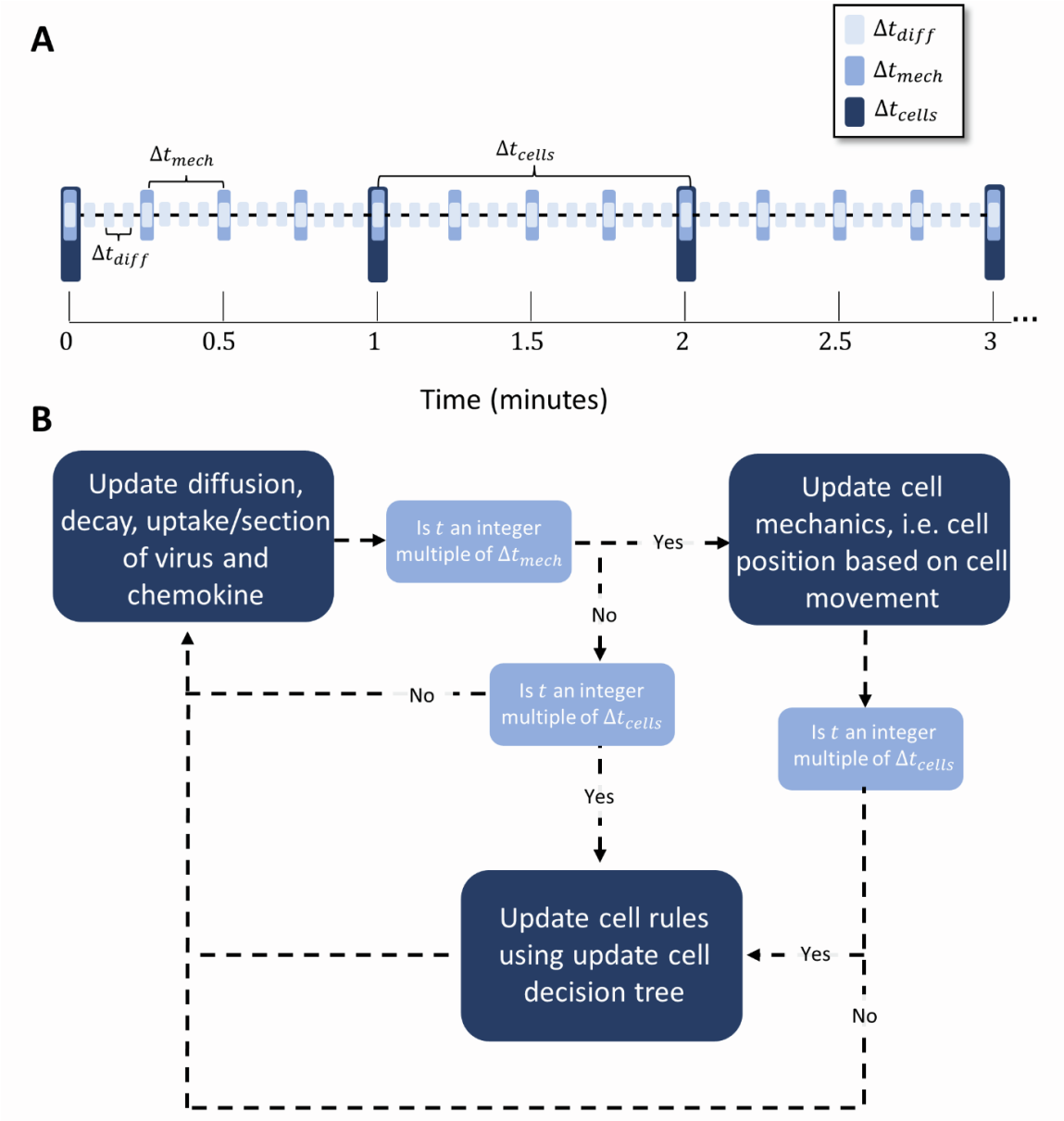

Figure S1. Summary of the time scales in PhysiCell and the overarching model evolution, related to Table 1. (A) PhysiCell uses multiple time scales or time steps to update the model. To update diffusion, decay, uptake and secretion of substrates in BioFVM, it uses the Δt_{diff}. Δt_{mech} is used to update cell mechanics (including cell positions). To update cell volume, death, infection, it uses Δt_{cell}. This image is a recreation of the original image summarizing these time steps published by Ghaffarizadeh et al. (2018). Note the time-scales depicted here are not the true time scale values used in the simulation and were chosen to as to demonstrate the evolution of the algorithm. The true time steps can be found in the **STAR Methods.** (B) A decision tree that complements the schematic in (A), depicting how the computational algorithm checks whether given the current time t it should update only the diffusive processes of virus and chemokine, or whether it should also update the cell mechanics (cell movement) and/or cell rules. The decision tree the algorithm follows when updating the cell rules can be found in **Figure S2**.

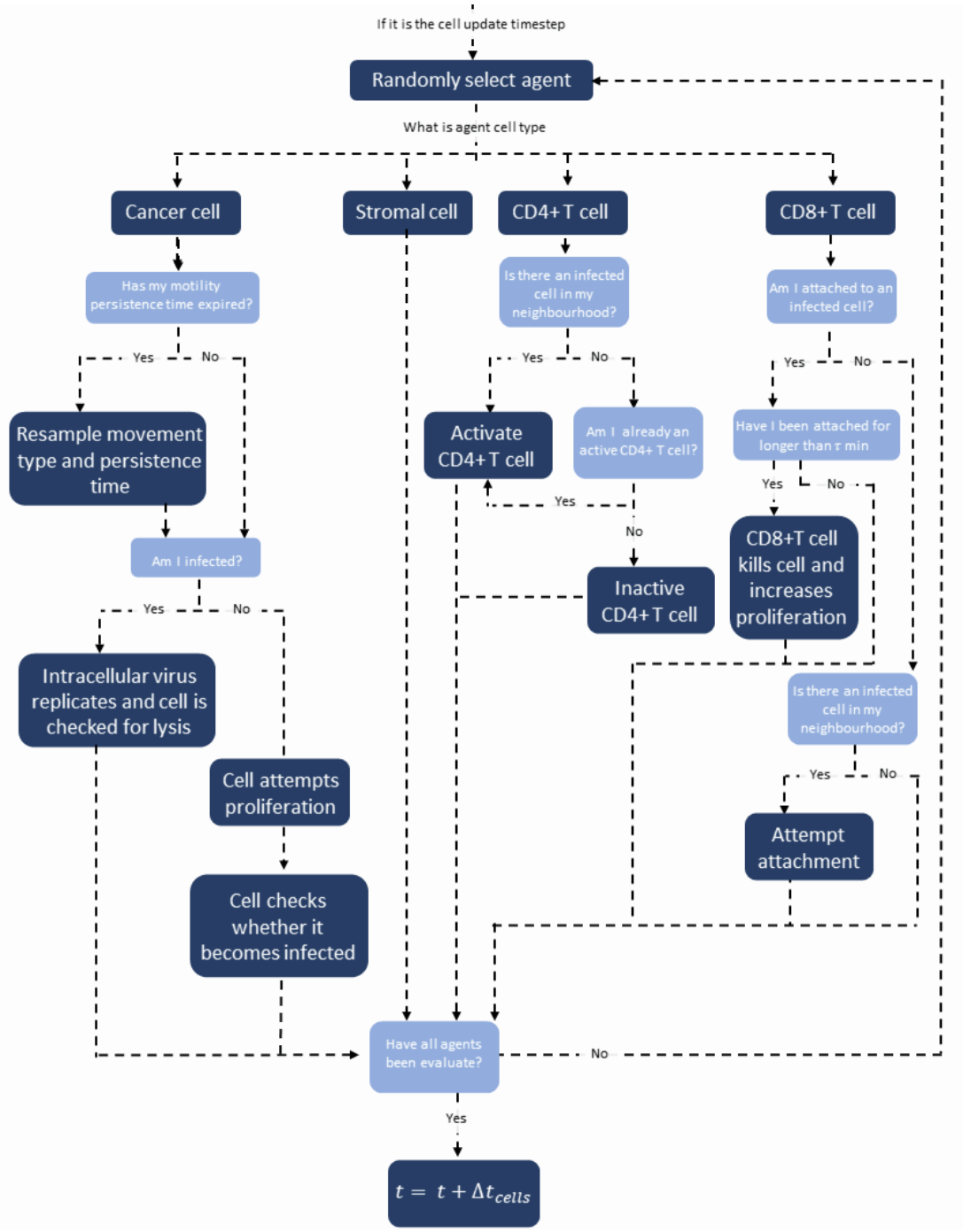

Figure S2. Decision tree for the cell update time step Δt_{cell}, related to Table 1. When the model has reached a time t that is a multiple of the cell update time step Δt_{cell}, the cells are updated. To update cells the process in the tree is followed. See **Figure S1** For details on how this time step relates to the diffusion and the diffusion time step and cell mechanics time step Δt_{diff} and Δt_{mech}. These times steps and their integration and built into the PhysiCell software and more details can be found at Ghaffarizadeh et al. (2018) or in the **STAR Methods**.

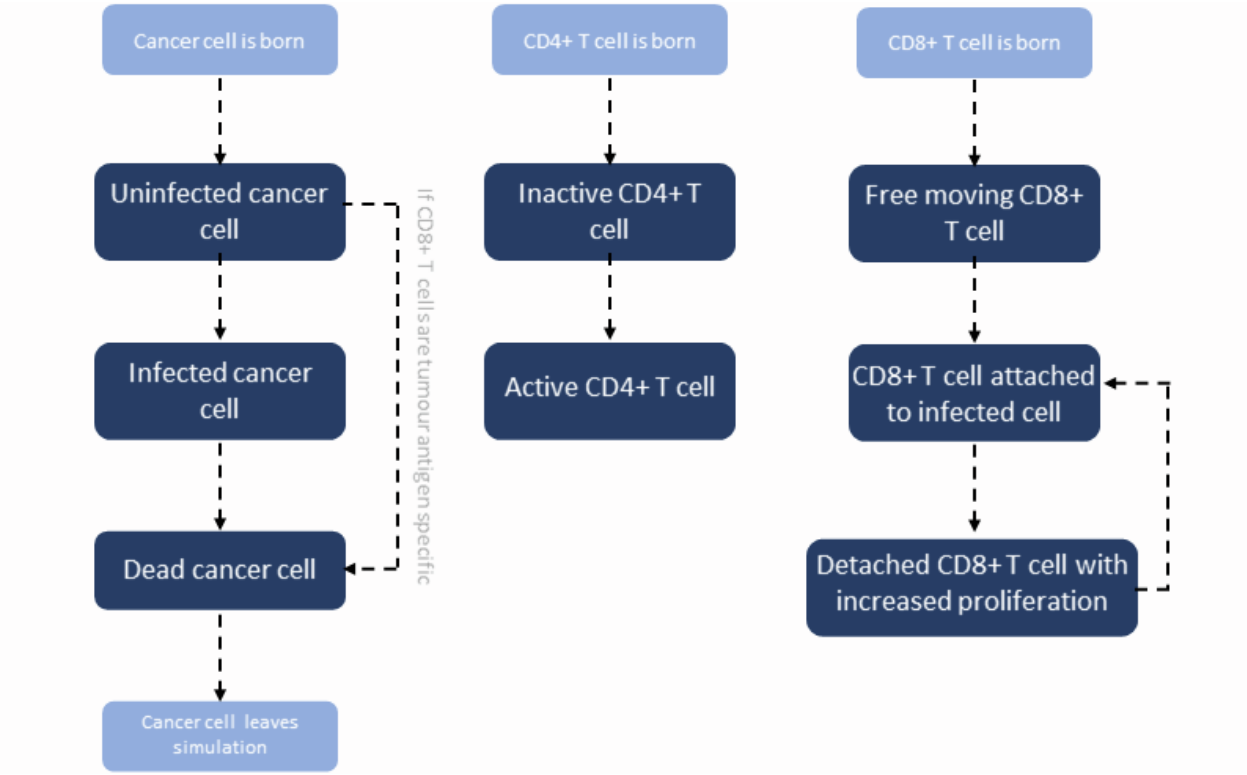

Figure S3. Hierarchy for cell types and their phenotypes in the model, related to Table 1. Cells move through stages dependent on environment stimuli. Cancer cells start as uninfected cancer cells. They can then become infected and die or if CD8+ T cells are tumour antigen specific they can die without becoming infected. CD4+ T cells start inactive and then become activated by infected cells. CD8+ T cells start off as free-moving cells, they then attach to infected cells and detach. After detaching they increase their proliferation and then can reattach to another infected cell.

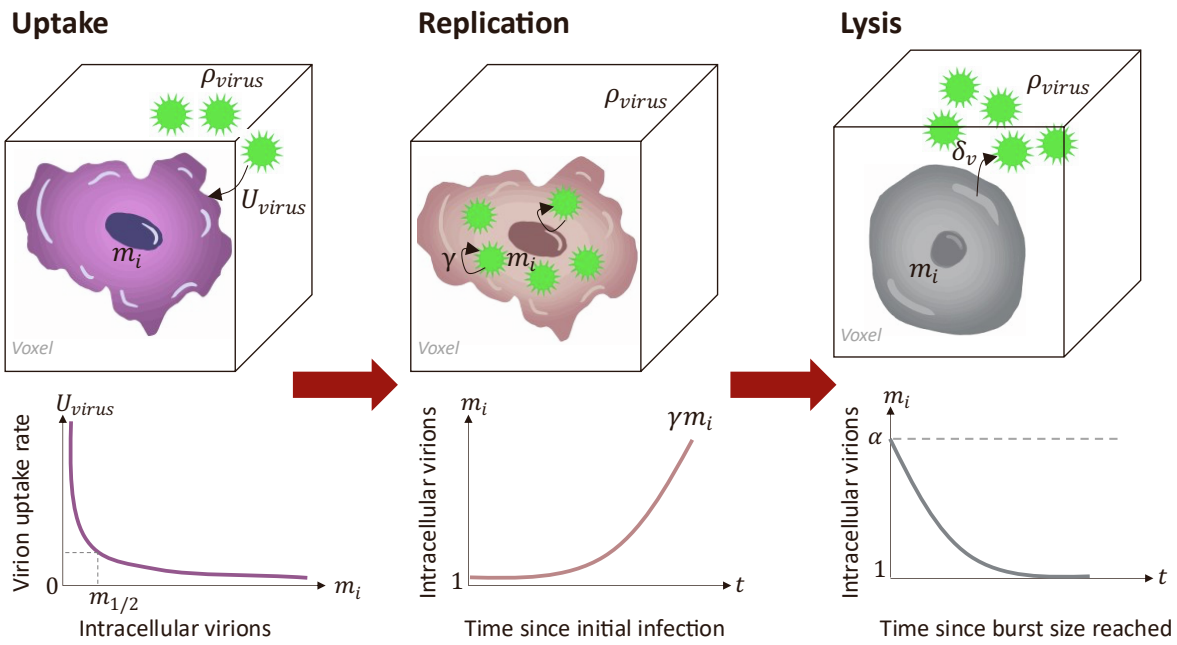

Figure S4. Schematic describing the intracellular virus model, related to Figure 2. Extracellular virus was modelled to be bound and internalised into the i^{th} cell based on the local voxel concentration of virus p_{v_i} and the amount of intracellular virus m_i. The virus then replicates within the cell at a rate γ proportional to the concentration of virus in that cell before undergoing lysis once the intracelluar concentration of virus exceeds α. Intracellular virus is then secreted into the extracellular domain at rate δ_V. Further details of the model and equations can be found in the **STAR Methods**.

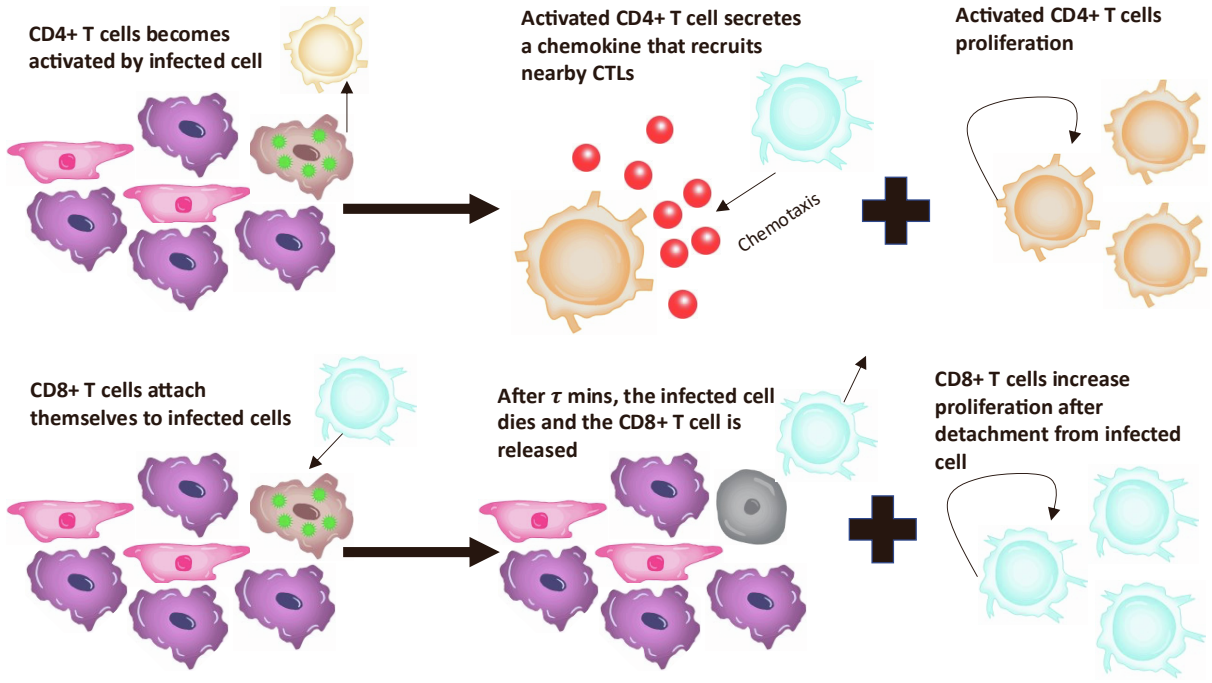

Figure S5. Model of the CD4+ and CD8+ T cells interactions and stimulation by infected cells, related to Figure 2. CD4+ T cells become activated if there is an infected cell in their neighbourhood of radius R_{TH} (**Figure S24**). They then secrete a cytokine, which we call the CD4+ T cell chemokine, at rate ψ_{TH} and which then diffuses at a rate D_{TH}. CD8+ T cells chemotaxis towards high concentrations of this cytokine and kill an infected cell if they are within $50\mu m$ of that cell.

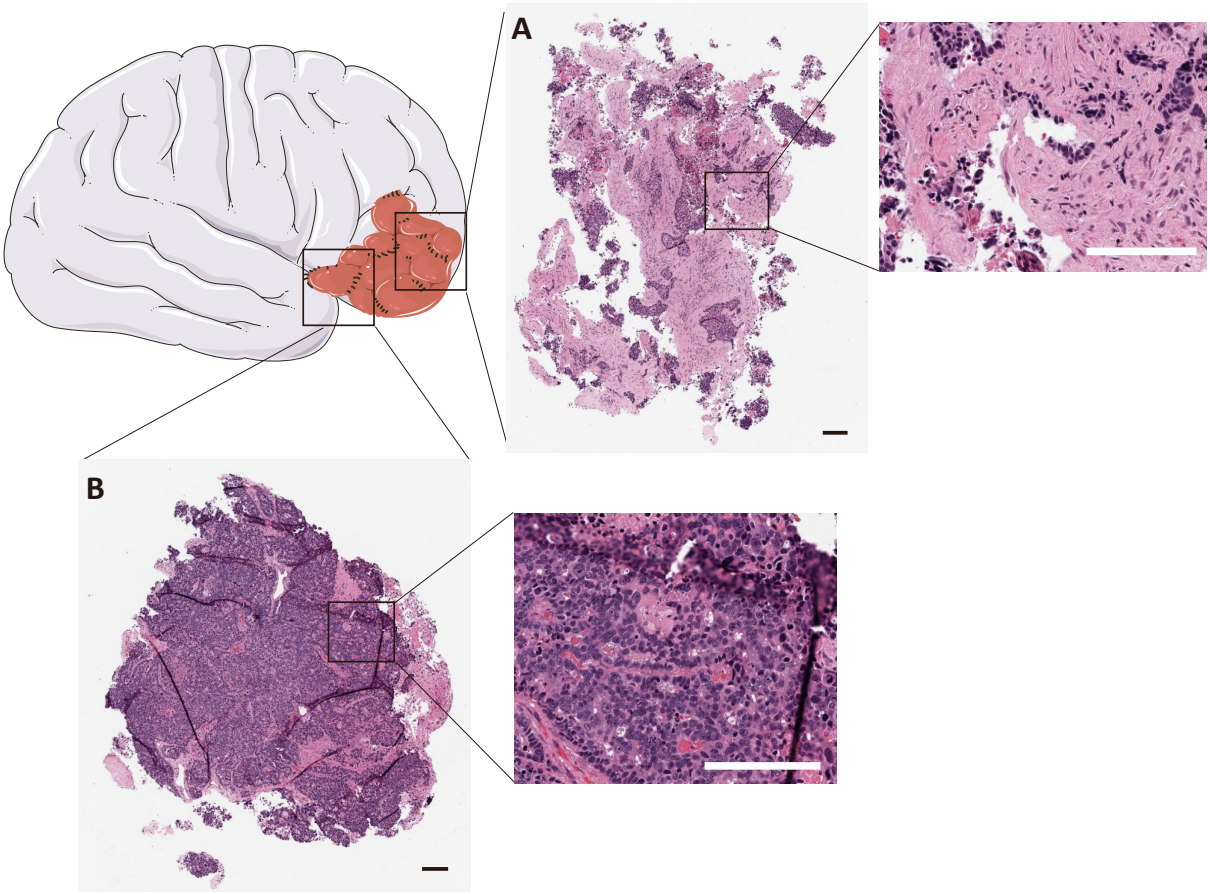

Figure S6. Zoomed inserts of patient-derived resected glioblastoma from Figure 2B (main text), related to Figure 2. A patient-derived resected glioblastoma was sub-sectioned into two smaller slices, which were then formalin fixed, paraffin embedded, sectioned onto slide, and stained with hematoxylin and eosin (H&E). Scale bar full image $= 750\mu m$, scale bar of inset $=120\mu m$. Stained purple cells are glioblastoma tumour cells and stained pink regions denote non-cancerous tissue (or stroma). A clinical pathologist scored the fraction of tumour cell, necrosis, immune cell, and stroma content (**Table 2** Main Text).

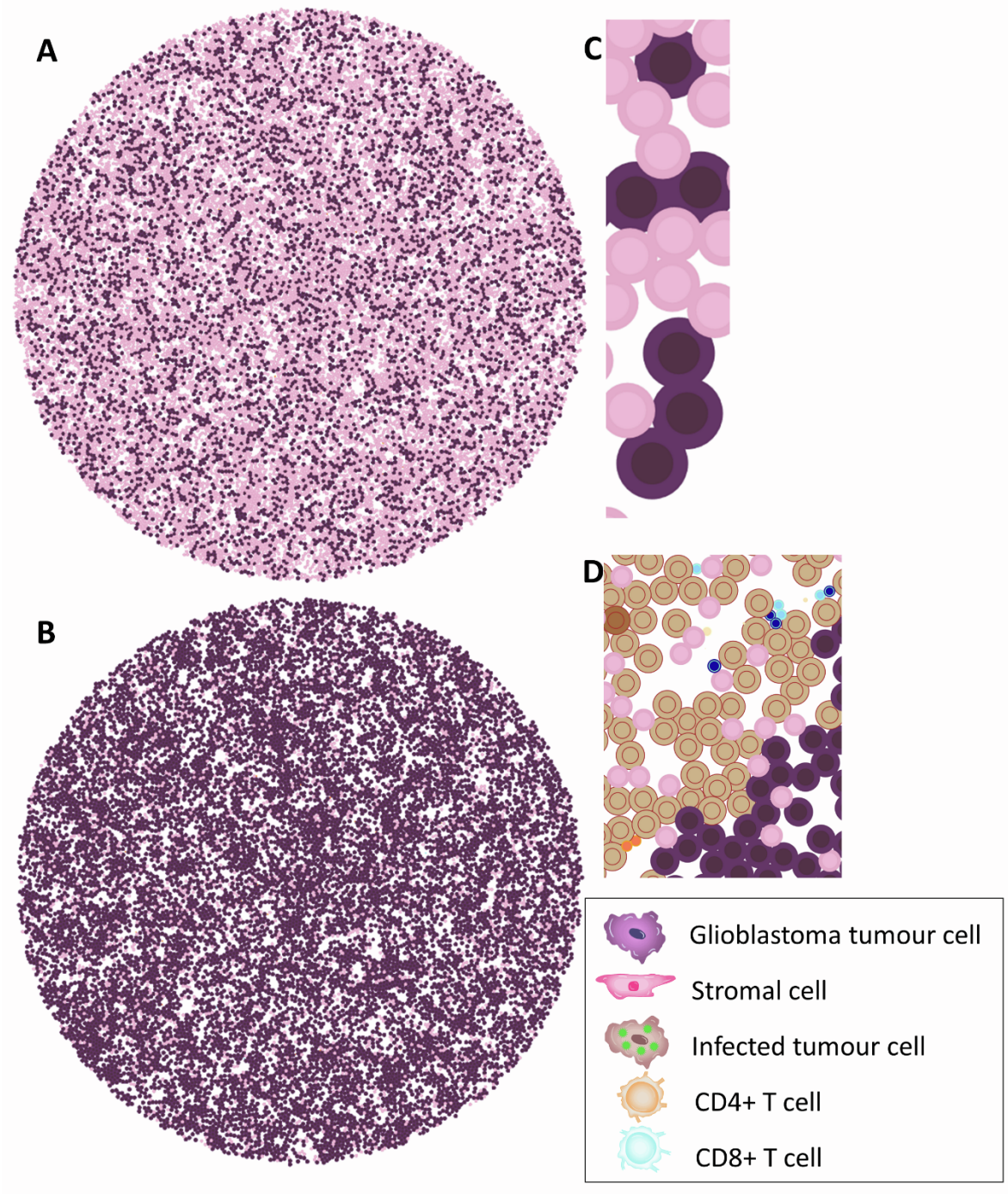

Figure S7. Close up of the sparse and dense fragment configuration, related to Figure 2. (A) Sparse and (B) dense fragments informed by pathologist scores (**Table 2** Main Text) with the number of stromal cells and glioblastoma cells in each fragment calculated using the cross-sectional area of cells and the percentage of the fragment designated by the pathologist as tumour cells. Pink cells: stromal cells; Purple cells: glioblastoma cells. These are reproductions of **Figure 2**B. (C) Close up of the cells in the sparse fragment. (D) Immune cell action during infection for CD4+T cells (orange) and CD8+T cells (blue). Dark and light colouring correspond to whether the cells are proliferative (Ki67+) or non-proliferative (Ki67-).

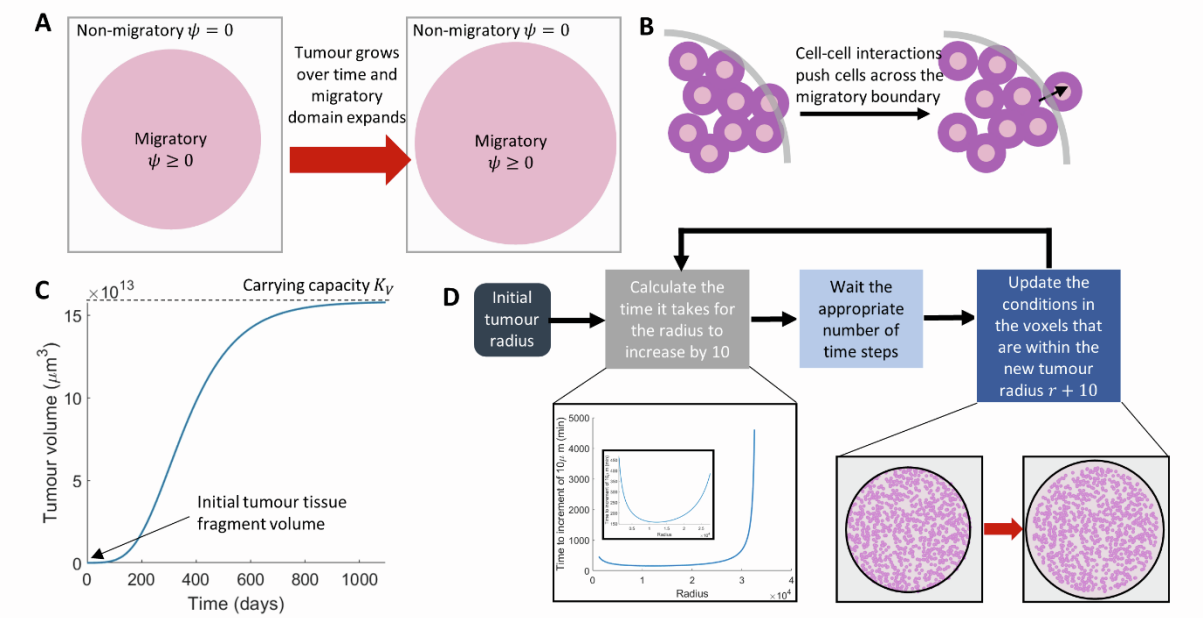

Figure S8. Migratory and non-migratory domain expansion, related to Figure 2. (A) Illustration of the subdivision of the domain into migratory and non-migratory areas. We expanded the tumour boundary over time to allow for the motility area for the cells to increase. (B) At the migratory boundary, glioblastoma and stromal cells were modelled as being pushed into areas where the motility is zero and, once there, they unable move again unless pushed. As the boundary expands, cells in an area previously designated non-migratory are able to migrate again. (C) From the initial fragment size, the Gompertz growth with parameters matched to MRIs of glioblastoma growth Stensjøen et al. (2015) and (2018) shows slow initial growth that takes about 3 years to reach carrying capacity. In our simulations, we used the initial growth to approximate the expansion of the fragment's radius by changing the migratory and non-migratory domains (A). (D) For a given initial tumour radius R, we calculated the time to each $10\mu m$ increase in the tumour boundary $t_{\Delta r=10\mu m}$ and then updated the radius of the non-migratory boundary.

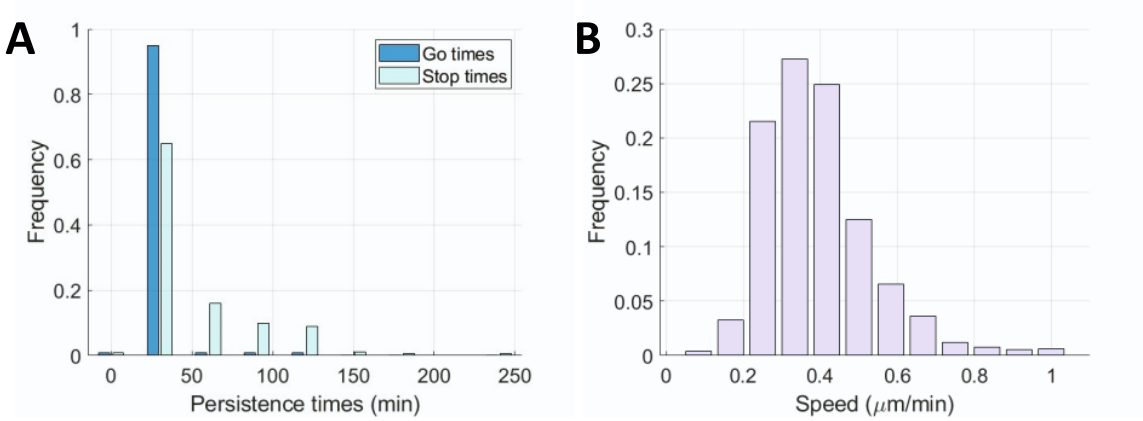

Figure S9. Extrapolating the distributions for glioblastoma cell speed and persistence time from Gallaher et al. (2020). related to Table 1. (A) The distribution for the persistence time T of cells that are moving ("go cells") and cells that are not moving ("stopped cells"). (B) The distribution for the speed of glioblastoma cells in the population. The data was reproduced from Gallaher et al. (2020) combining their phenotypic distributions.

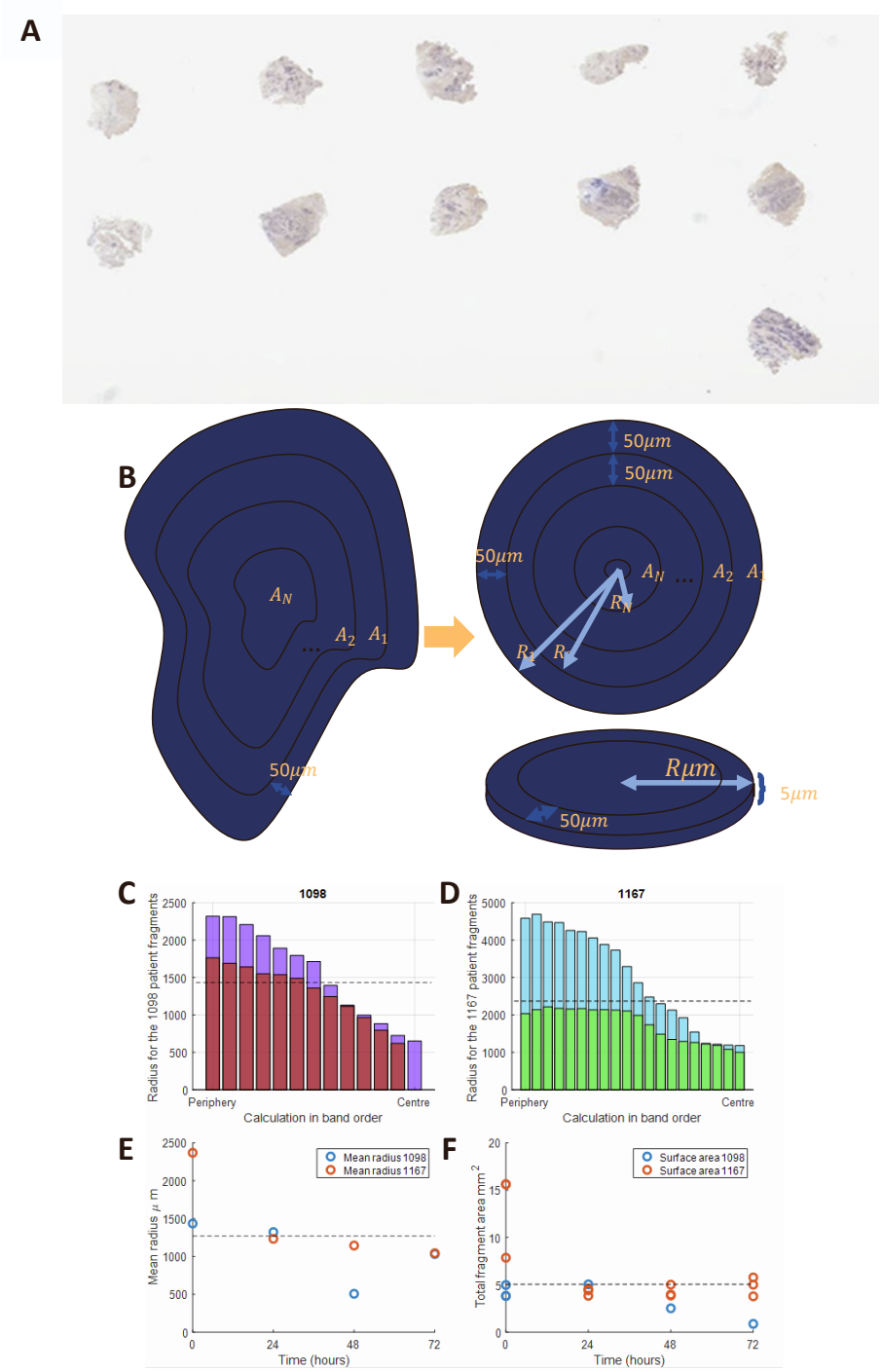

Figure S10. Extrapolating tumour slice radius from HALO measurements, related to Figure 3. (A) Selection of images of $5\mu m$ thick tumour slices obtained from our CANscript samples (**Figure 1** Main Text). (B) Schematic representation of the domain and area circular approximation for the slices. Bands $50\mu m$ thick are denoted in from the periphery and used by HALO to measure fragment dimensions. The area $A_i\mu m^2$ of the ith band is used to determine the radius $R = R_1\mu m$ of the slice. (C)-(F) An approximation for the radius of each slice (R_1) was calculated using the area of the ith band, $A_i\mu m^2$ (B) for (C) patient 1098 ($n = 2, t = 0$), and (D) patient 1167 ($n = 2, t = 0$). The different coloured bars represent different slices for each patient. The combined mean radius across all samples was $2009.8\mu m$. Dotted line: mean radii for slices 1098 and 1167. Repeating this calculation for both patients control slices at 0, 24, 48 and 72 hours gives (E) the mean radius and (F) the total surface area. Each circle represents a distinct slice and the dotted line is the mean.

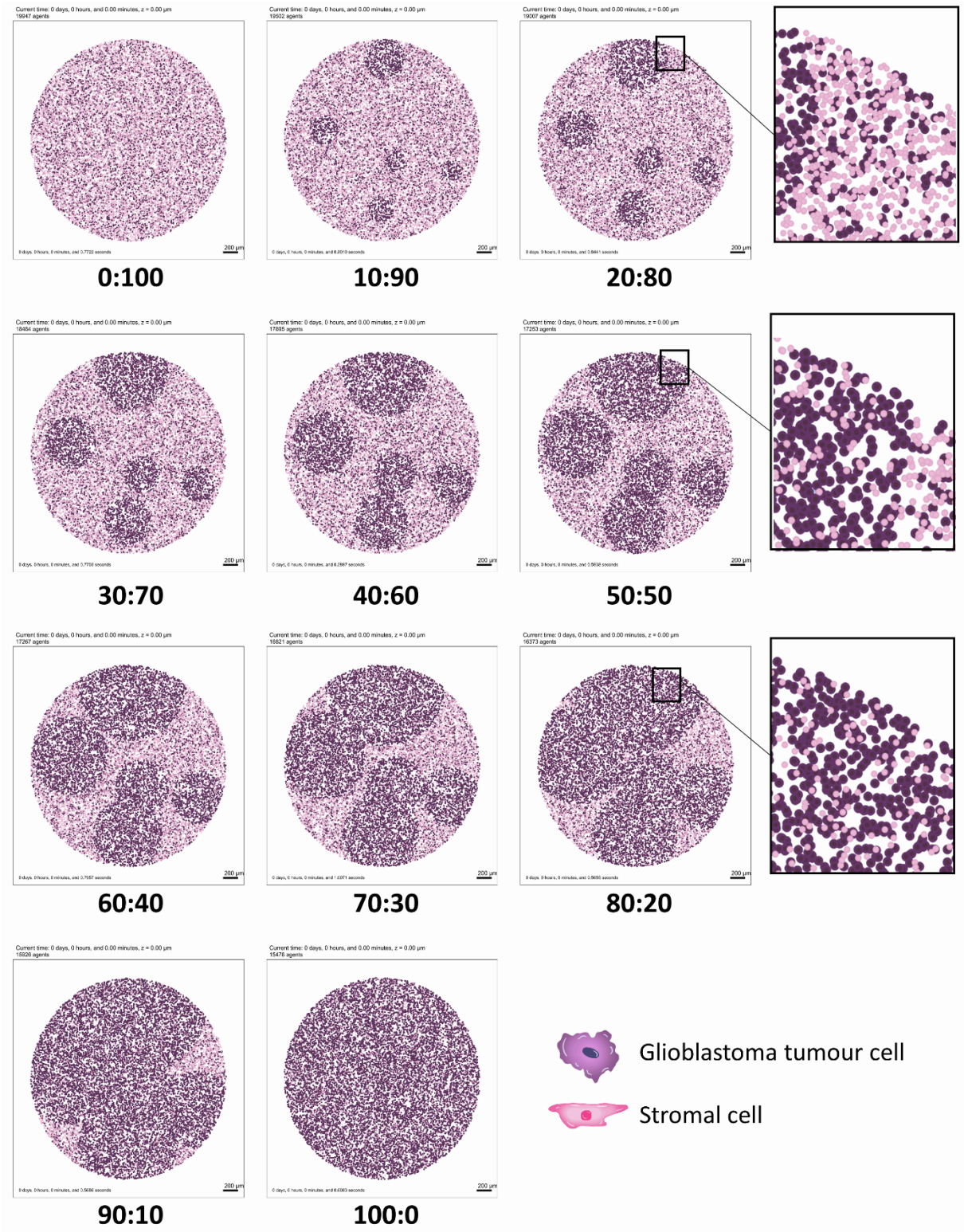

Figure S11 Spatial configurations for the dense:sparse tumour tissue, related to Figure 4. Using clinical pathologist scores for patient-derived glioblastoma tissue (**Figure 2**B) we generated a configuration of tumour cells to stromal cells that make up a 'dense' sample and a 'sparse' sample (**Table 2**). In the above, a dense tumour tissue corresponds to 100:0 and a fully sparse tumour tissue corresponds to 0:100.

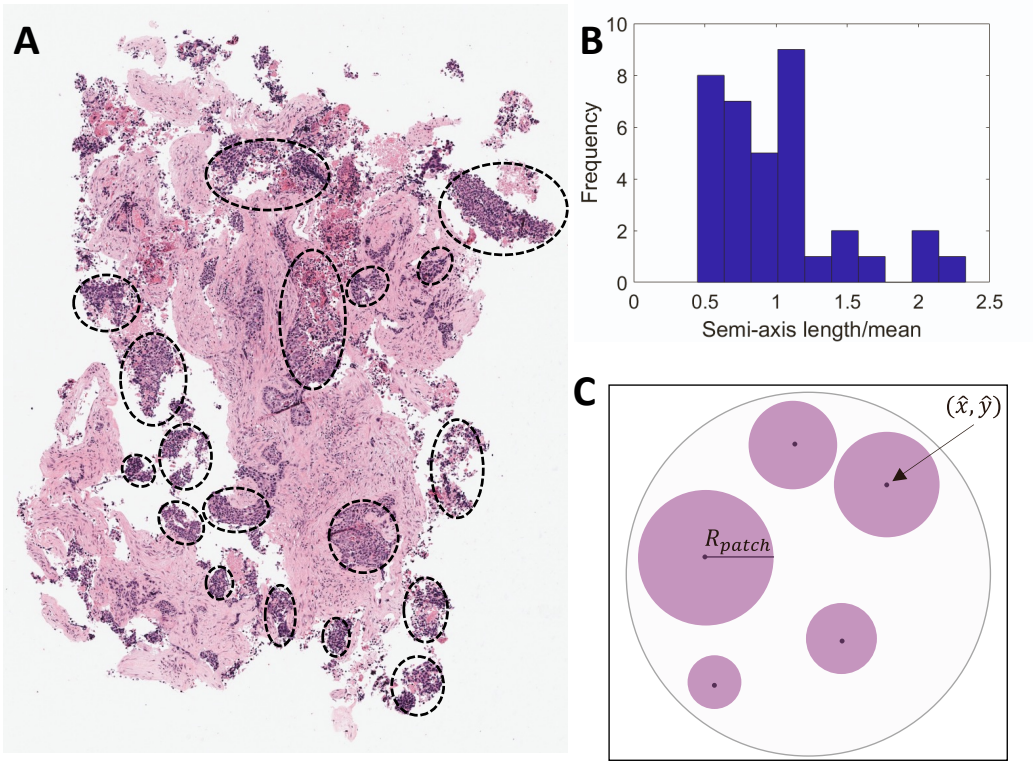

Figure S12. Generating patchy slices consisting of dense & sparse regions, related to Figure 4. (A) Patient-derived glioblastoma tumour slice stained for stromal cells (pink) and glioblastoma cells (purple). Sections of dense glioblastoma cell populated areas were approximated with ellipses (black dashed lines). (B) Histogram of the normalized semi-axis lengths of the ellipses denoted in (A). The normalized semi-axis lengths were determined by dividing each semi-axis by the average of all the semi-axis measured. (C) Schematic describing the generation of patchy tumours. The centre of patches $(\hat{x}, \hat{y})$ were determined by sampling from a uniform distribution for the distance and angle from the patch centre. The radius of each patch R_{patch} was then determined by sampling from a normal distribution inferred from (B).

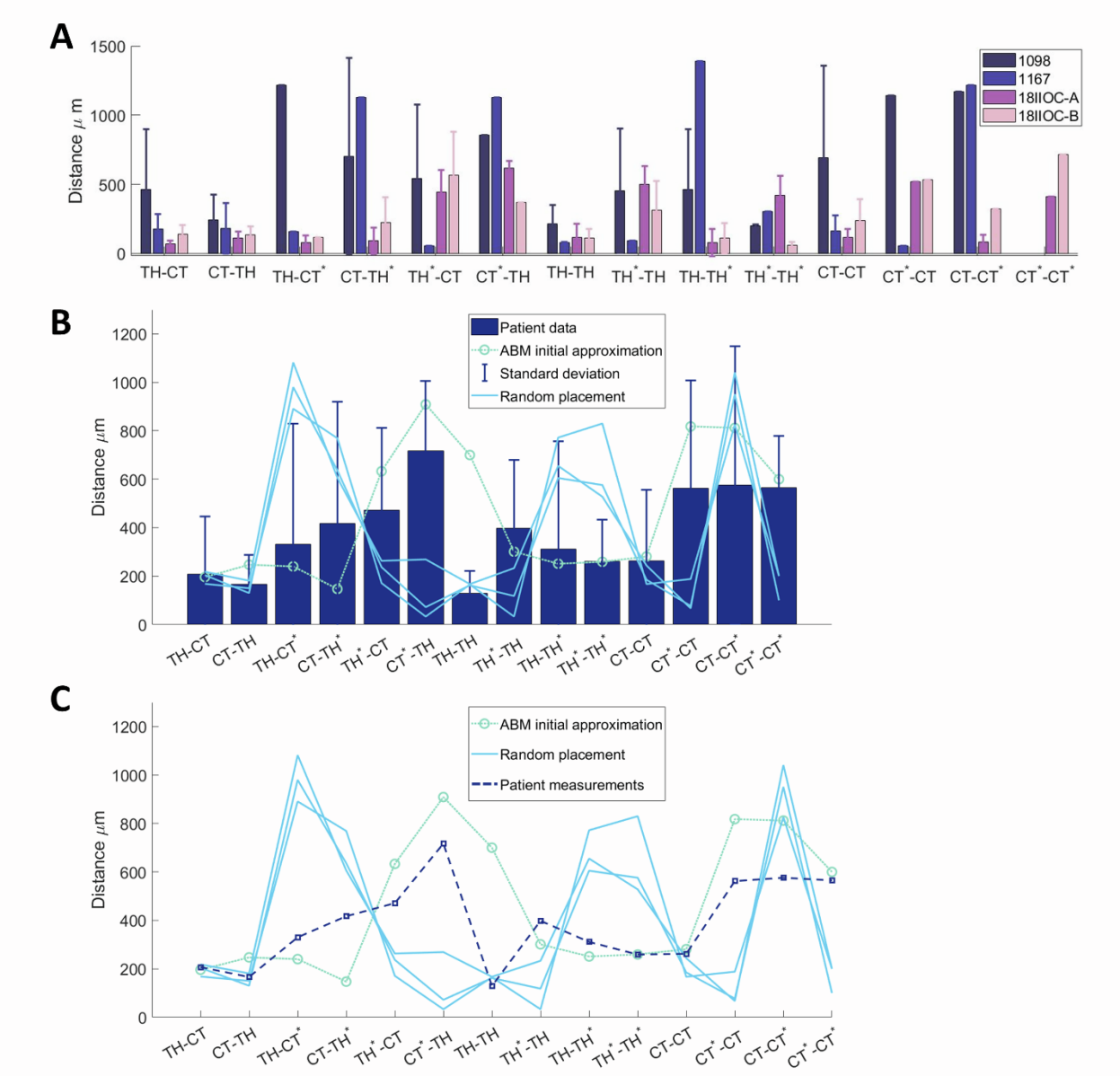

Figure S13. Nearest neighbour distances between CD4+ (TH) and CD8+ (CT) T cells in patients 1098, 1167, 18IIOC-A and 18IIOC-B, related to Figure 3. (A) Histogram of each cell-cell relationship for each patient (1098, 1167, 18IIOC-A and 18IIOC-B). Ki67+ proliferative (*) and Ki67-non-proliferative subsets of cells were noted and for each cell-cell pair relationship, the distance from a randomly chosen cell of the first type to its nearest neighbour of the second type was calculated. Error bars for the standard deviation in the immune cell distances across all patient slices where patient1098 had n = 20, patient 1167 had n = 20, patient 18IIOC-A had n = 23, and patient 18IIOC-B had n = 18. Histogram of mean cell-cell distance relationship across all patient slices is given in **Figure 3**B. TH: CD4+ T; CT: CD8+ T cells. Proliferative (Ki67+) are denoted by * (B)-(C) Comparison of nearest neighbour distances from the Hooke's law simulation with random initial placement. Three instances of random initial placement have been plotted where the nearest neighbours were measured and averaged. The single iteration of Hooke's law from (A) and **Figure 3B** in the main text is overlaid as well as the patient data average. The plots in (C) and (D) are recreations of each other with and without the standard deviation and with the bar graph replaced by a line plot.

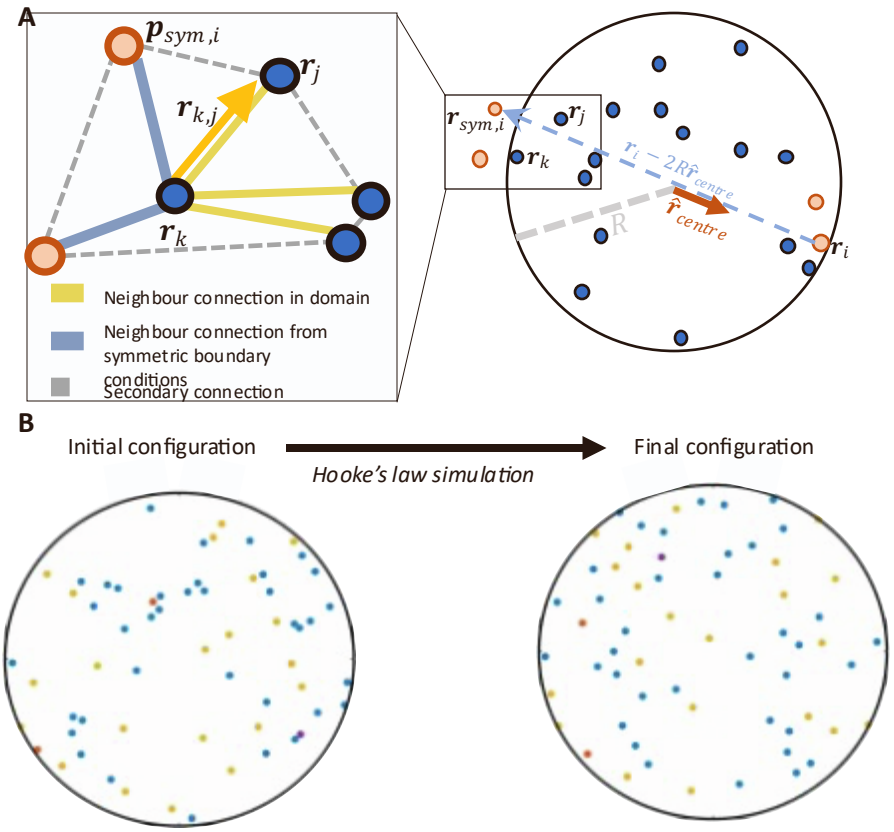

Figure S14. Simulating Hooke's law to determine initial spatial configuration of CD4+ T cells and CD8+ T cells, related to Figure 3. (A) Schematic for the ABM model that provides the initial distribution of immune cells. For a point $\boldsymbol{r}_k$, the nearest neighbours are determined using a Delaunay triangulation. The vector $\boldsymbol{r}_{k,j}$ is the vector connecting point $\boldsymbol{r}_k$ with its neighbour point $\boldsymbol{r}_j$ and is used to calculate the movement of this point governed by Hooke's law (**Eq. 3**). In this scenario, the point $\boldsymbol{r}_k$ is close to the boundary, and so has neighbour points which arise due to symmetric boundary conditions (i.e.. $\boldsymbol{r}_{sym,i}$). All points within the circle have a duplicate point outside the circle that is located diagonally on the exterior of the circle and used as part of the Delaunay triangulation. (B) The resulting configuration of THs (blue), THs* (orange), CTs (yellow), CTs* (purple) after the Hooke's law simulation, where the stopping criterion was that the distance cells have moved in Δt is less than $5\mu m$. For the average minimum distance between each cell type TH, TH*, CT and CT* after a single simulation of the Hooke's law simulation see **Figure 3**B.

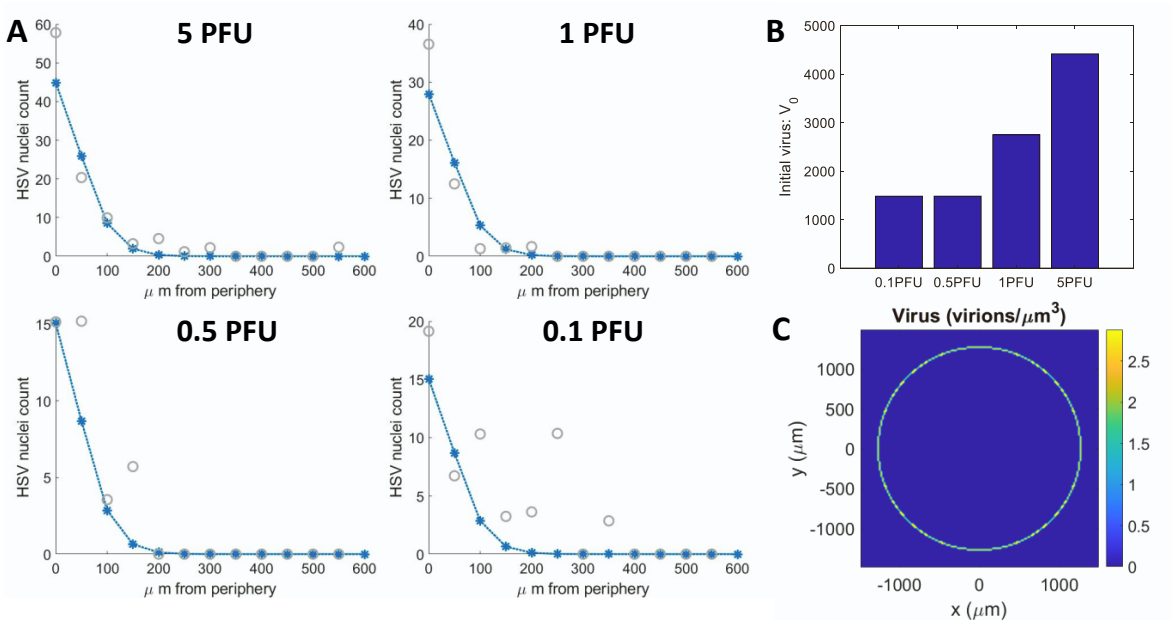

Figure S15. Fitting extracellular viral diffusion and decay to GFP infiltration measurements, related to Figure 3. (A) HSV nuclei counts measured at 24 hours for 5 PFU, 1 PFU, 0.5 PFU, and 0.1 PFU. **Eq. 6** was fit to these measurements by assuming the initial size of the viral population varied between the different PFU experiments but that the diffusion coefficient (D_{virus}) and the decay rate (λ_{virus}) were fixed across the different experiments. Grey circles: observed data. Dotted blue line: Model fit. Stars: Model prediction at the equivalent band at a given distance from the periphery. (B) Bar plot for the different initial virus PFUs obtained from the fit to the different PFU. (C) Initial virus density at the edge of the tumour slice, estimated using **Eq. 1** at 5 PFU.

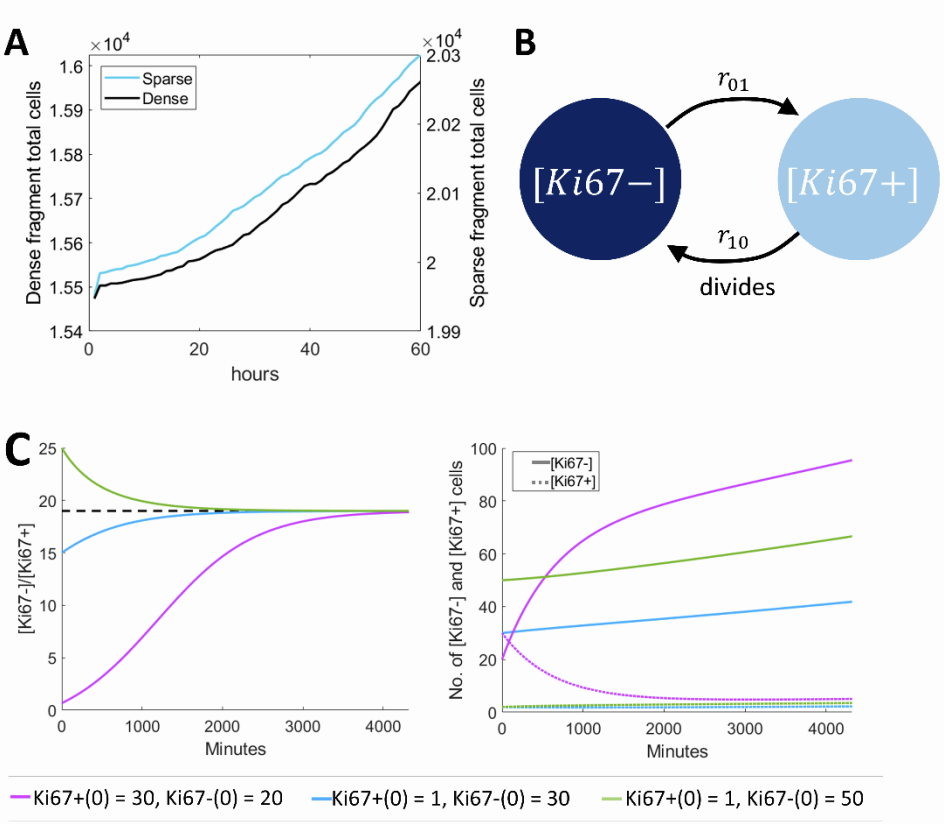

Figure S16. Glioblastoma, Ki67+ and Ki67- cell growth in the model, related to Figure 3. (A) Glioblastoma tumour cell numbers in dense (black) and sparse (blue) tumour slices over time predicted from our PhysiCell model simulation without virus. Parameter values for the proliferation of glioblastoma cells are in **Table S2** and were obtained by fitting to cell count measurements from Mercurio et al. (87) (**Figure 3**C Main Text)**.** (B) The Ki67 Basic proliferation model inbuilt in PhysiCell. In this model, cells are either in a non-proliferative (Ki67-) or proliferative (Ki67+) state. Cells transition from a non-proliferative to proliferative state at a rate r_{01} and cells transition from a proliferative to a non-proliferative state and divide at a rate r_{10}. (C) For different initial conditions, the ratio of non-proliferative (Ki67-) and proliferative (Ki67+) cells (left) and the explicit number (right) were plotted. The different initial conditions are given in the legend and correspond to different line colours. The number of Ki67- and Ki67+ cells (right) are represented by a solid and dashed line, respectively. These plots summarise the stable nature of the T cell proliferation model.

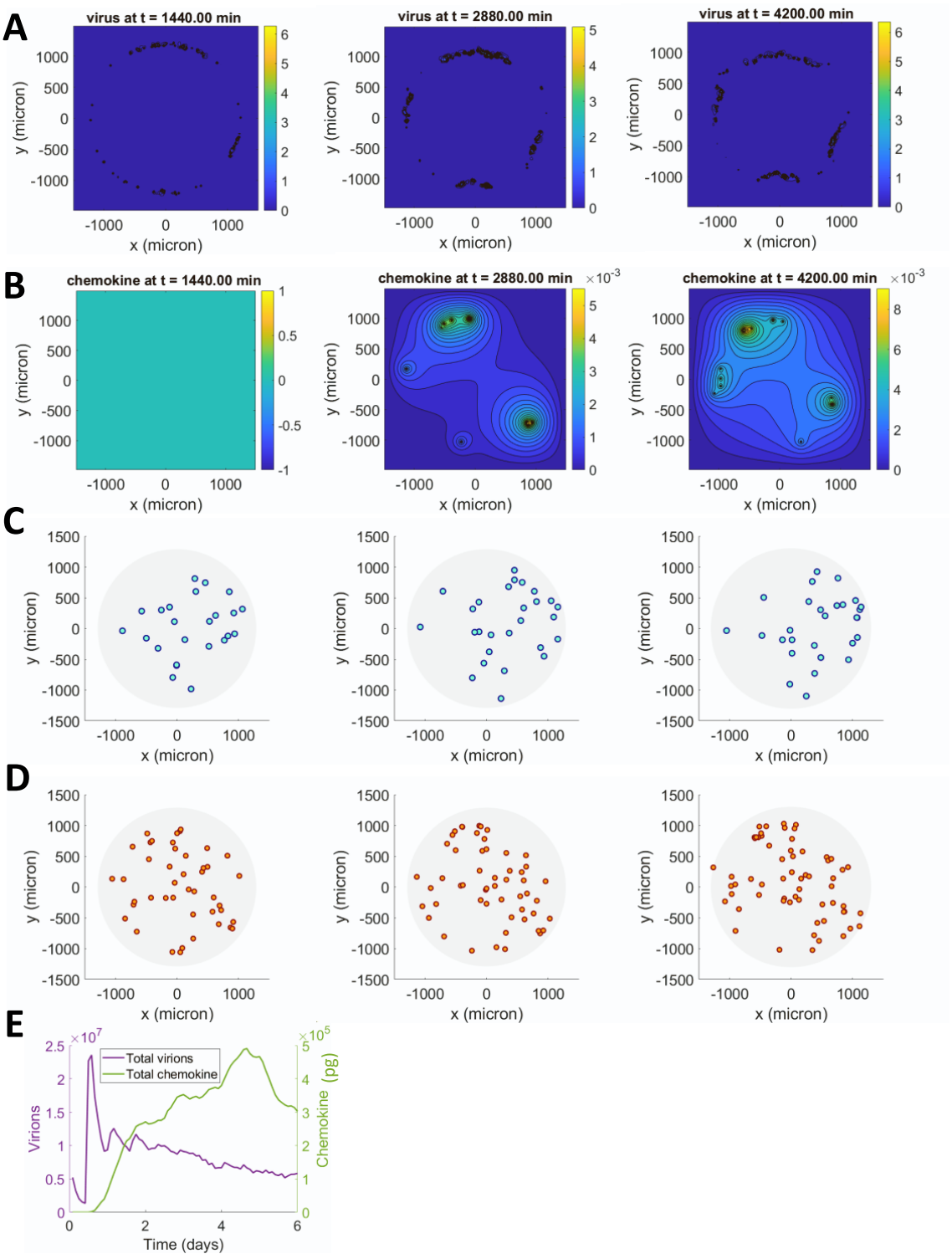

Figure S17. Density of chemokine and extracellular virus (patchy tumour slices with 50% dense and 50% sparse regions), related to Figure 4. Contour plots for the spatial density of (A) extracellular virus and (B) chemokine at Left: 24 hours, Middle: 48 hours, and Right: 72 hours. Corresponding location of (C) CD8+T cells and (D) CD4+T cells at Left: 24 hours, Middle: 48 hours, and Right: 72 hours. (E) Total virions and chemokine (pg) in the tumour slice over 6 days.

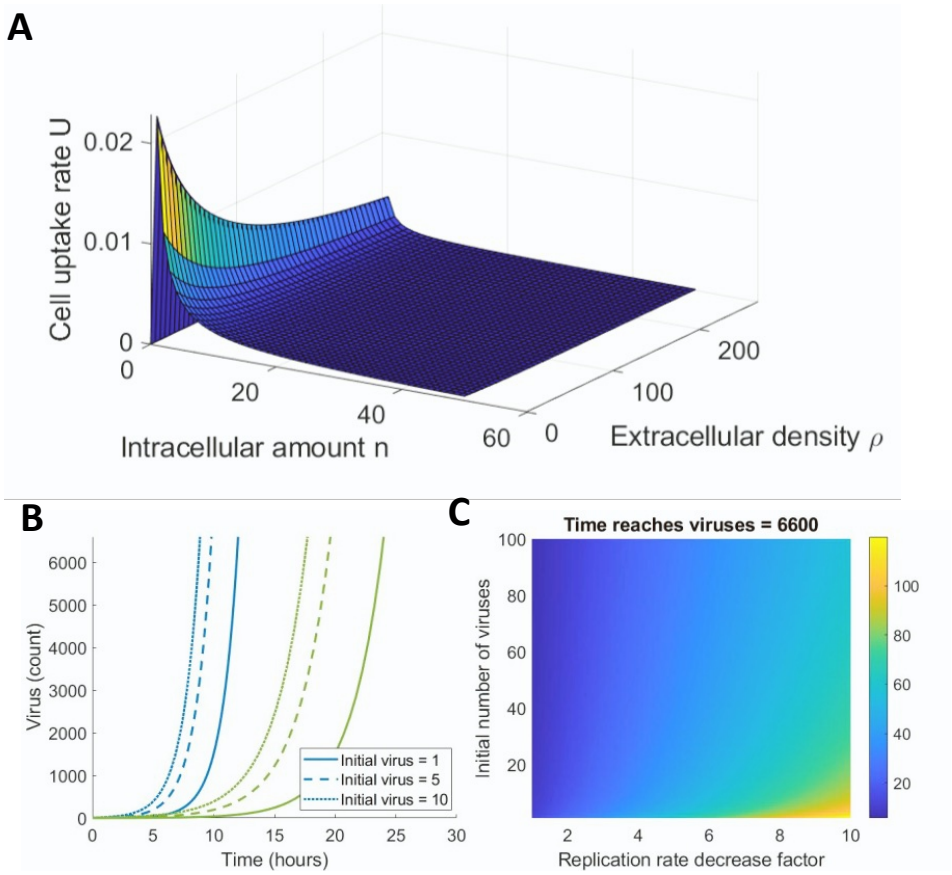

Figure S18. Exploration of the viral binding and replication models, related to Figure 2. (A) The binding rate of the virus for each cell as a function of the intracellular amount of virus within that cell $m(t)$ and the extracellular density of virus $\rho(t)$ (**Eqs. 10-11, STAR Methods**). (B) and (C) Intraceullar viral counts for different initial virus infections ($m_i(0) = 1, 5, 10$) with virus replicating according to **Eq. 9**. (C) The impact of decreasing the replication rate on the time taken to reach 6600 intracellular virions.

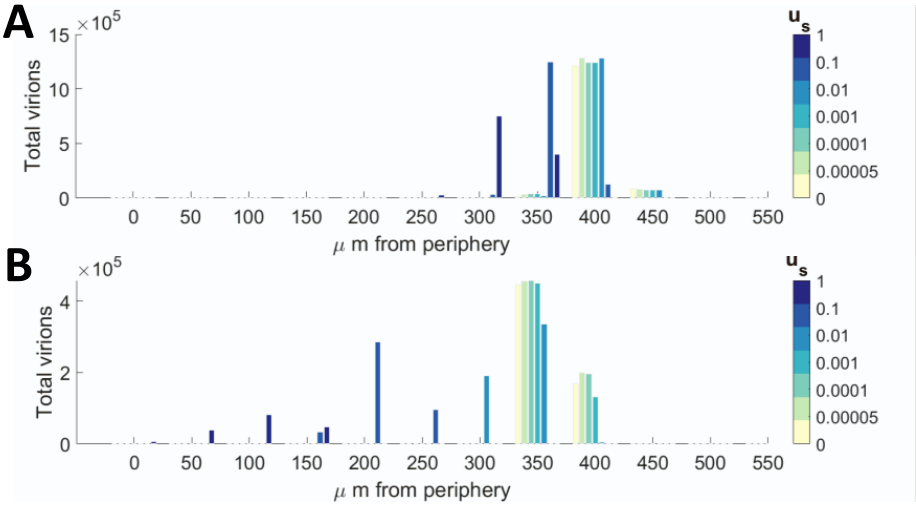

Figure S19. Increasing the inhibition of stroma has a significant impact on infiltration in glioblastoma, related to Figure 6. The total intracellular virus in glioblastoma cells in 50μm bands after 72 hours at the given distance from the periphery of the tumour slice for different stromal-virus binding rates (u_s) in (A) dense and (B) sparse tumours. The colour of the bar corresponds to the stromal-virus binding rate. Corresponding percentage of tumour remaining is in **Figure 6**D in the Main Text.

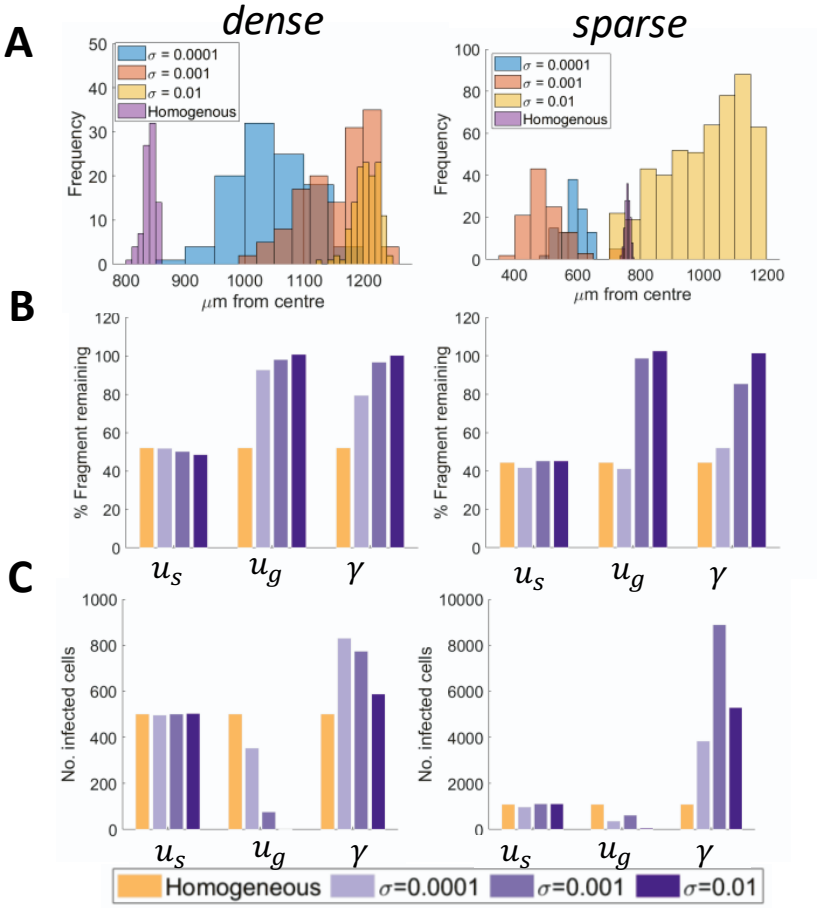

Figure S20. Impact of heterogeneity in viral replication and binding rates on viral infiltration and cell counts, related to Figure 6. Heterogeneity was introduced into parameters γ, u_s and u_g by assigning each cell a value drawn from a gamma distribution with mean as the original parameters value (i.e. $\gamma = 0.0081, u_s$ =0.01 and u_g =0.002) and variance $\sigma = 0.0001, 0.001.$ and 0.01 (A) Distance of infiltration (μm) of infected cells was measured in sparse and dense tumours for varying variances on the replication rate γ distribution. (B) Percent of the initial tumour slice remaining at 72 hours in sparse and dense tumours for varying values of the stromal cell binding rate u_s, glioblastoma cell binding rate u_g, and viral replication rate γ. (C) Corresponding number of infected cells to (B). Left column: results in dense tissue slices; Right column: results in sparse tissue slices.

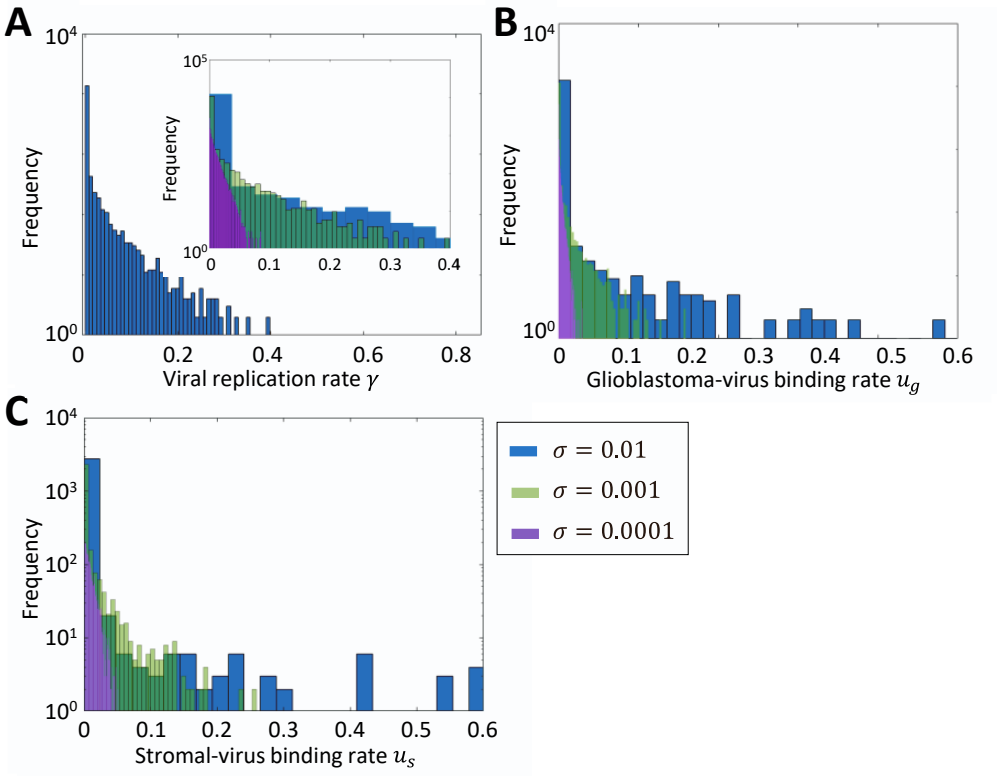

Figure S21. Corresponding gamma distributions for parameter values in Figure S8, related to Figure 6. Gamma distributions used to define parameter values: (A) viral replication rate γ, (B) glioblastoma cell binding rate u_g, and (C) stromal cell binding rate u_s. Histograms of the different parameters are given for variance $\sigma = 0.0001$ (purple), $\sigma = 0.001$ (green) and $\sigma = 0.01$ (blue).

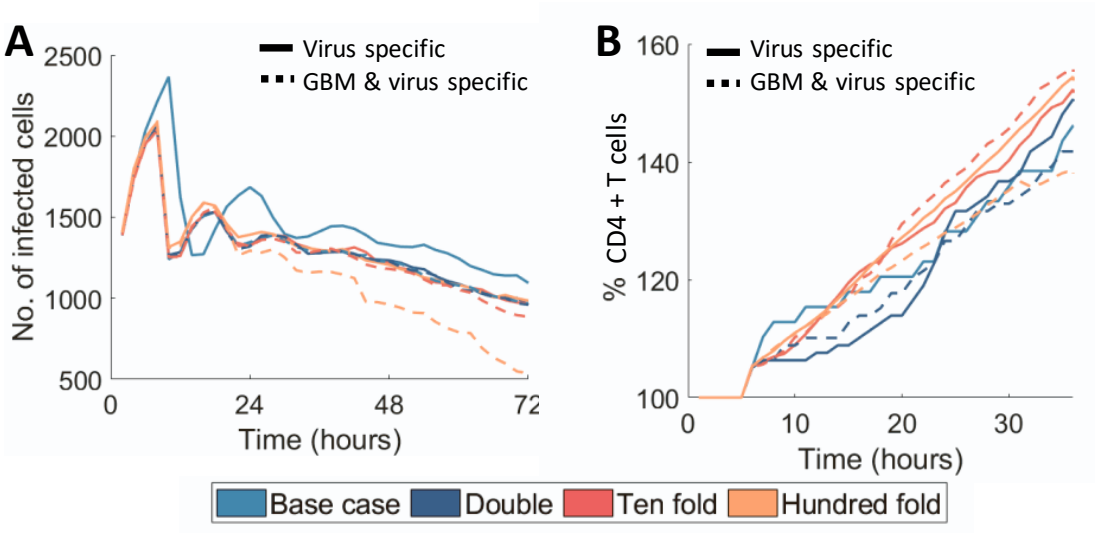

Figure S22. Infected cells over 72 hours with changes in CD8+ & CD4+ T cell numbers and antigen specificity, related to Figure 6. The number of CD4+ and CD8+ T cells was increased two-times, ten-times and one hundred-times from the base case. (A) Infected cell number and (B) CD4+ T cell number over time for varying immune cell multiplicities. The corresponding percentage of tumour remaining at 72 hours is given in **Figure 6**A in the Main Text. Virus-specific: CD8+ T cells induce apoptosis in infected cells only or glioblastoma; Virus specific: CD8+ T cells induce apoptosis in both uninfected and infected cells (see Main Text).

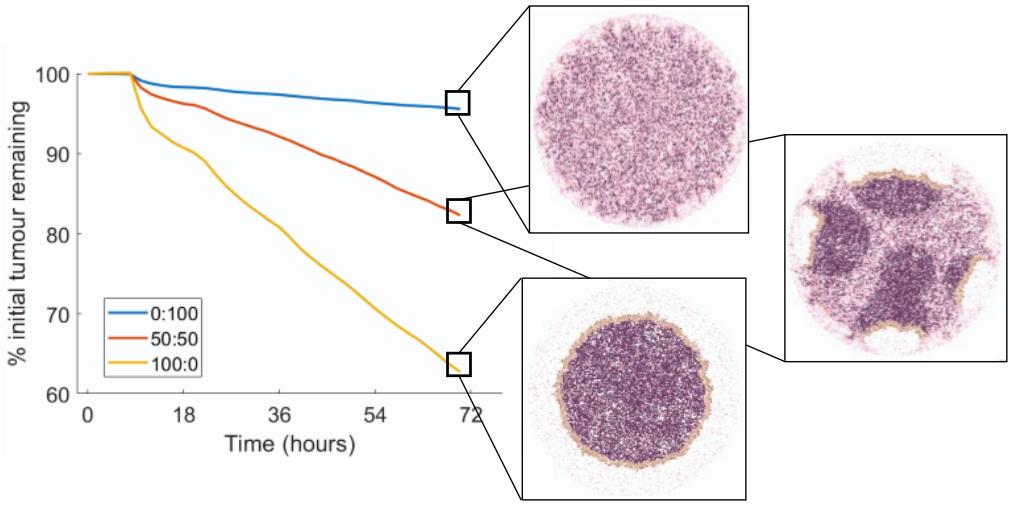

Figure S23. Predicting treatment efficacy on varying stromal densities, related to Figure 7. The percentage of the initial tumour slice remaining over 72 hours with corresponding model snapshot (for results in **Figure 7**A in Main Text). In these simulations, the stromal-virus binding rate was set as $u_s = 1$. Yellow curve: 100:0 dense:sparse; Red curve: 50:50 dense:sparse; Blue curve: 0:100 dense:sparse.

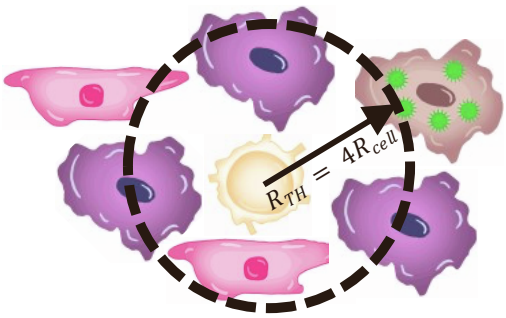

Figure S24. Estimating the neighbourhood and secretion rate of chemokine for CD4+ T cells, related to Figure 2. Schematic summary of the neighbourhood (Π) defined as the cells within a distance R_{TH} of a particular CD4+T cell.

Table S1. Values of the tumour slice area correction factor κ, related to Figure 4. Tumour slices were generated with dense and sparse regions in an area ratio of dense:sparse. The radius of each dense patch was scaled by κ to obtain the correct area ratio (**Figure S5**). The number of GBM cells (N_{GBM}) and stromal cells (N_{stroma}) for different rations of dense:sparse are also given above.

Density of tumour slice (dense:sparse)	Area correction factor (κ)	N_{GBM}	N_{stroma}
10:90	0.4080	5641	14306
20:80	0.5922	6402	13100
30:70	0.7380	7100	11907
40:60	0.8625	7797	10687
50:50	1.000	8495	9400
60:40	1.088	9192	8584
70:30	1.208	9890	7377
80:20	1.350	10589	6232
90:10	1.568	11285	5088

Table S2. Model parameters and variables, related to Table 1. All relevant model parameters and variables are summarized below. For parameters with a fixed value, their value has been noted below, and remaining variables or un-fixed parameters have been noted in the second table with the size of vectors. The reference for each parameters value is given.

Symbol	Units	Description	Value	Ref (see Main Text)
A_{frag}	mm^2	Total area of tumour slice	5.0644	**Figure S10**
α	virions	Virus burst size	6600	Lambright et al. (2000)
β	1/min	Tumour cell proliferation rate	7.35×10^{-4}	**Figure 3**C
c_j^{ccr}	μm/min	Cell-cell repulsive force coefficient	10	Macklin et al. (2012)
c_S	$\mu g/hour^2$	Spring constant	0.01	Jenner et al. (2020)
D_{virus}	$\mu m^2/min$	Diffusion coefficient for virus	1.4766	**Figure S15**
$D_{chemokine}$	$\mu m^2/min$	Diffusion coefficient for chemokine	555.56	Matzavinos et al. (2004)
d_{attach}	μm	CD8+ T to infected attach cell distance	50	Estimated
δ_V	1/min	Release rate of virus	0.1466	Nakashima et al. (2018), Lambright et al. (2000)

ϵ	μm	Length of voxel	20	Ghaffarizadeh et al. (2018) and (2015)
η	μm hour	Velocity of proportionality	0.133	Jenner et al. (2020)
f_F	dimensionless	Fluid fraction of the cell	0.75	Ghaffarizadeh et al. (2018)
γ	1/min	Virus replication rate	0.4886	Nakashima et al. (2018) and Lambright et al. (2000)
K_V	μm^3	Tumour volume carrying capacity	1.58×10^{14}	Stensjøen et al. (2015) and (2018)
K_C	cells	Tumour cell number carrying capacity	4.76×10^{6}	**Figure 3**C
λ_{virus}	1/min	Decay rate for virions	0.0029	**Figure S15**
$\lambda_{chemokine}$	1/min	Decay rate for chemokine	8.06×10^{-6}	Reisenberger et al. (1996)
$m_{1/2}$	virions	Infection threshold half-effect	10	estimated Lambright et al. (2000)
μ	μm	Average patch radius	402	**Figure S12**
N_{CD4}	cells	Number of CD4 cells	39	**Figure 3**A
N_{CD8}	cells	Number of CD8 cells	22	**Figure 3**A
v_{max}	μm/min	Maximum speed of CD8+ T cells	24.6	Bhat et al. (2017)
v^*	pg/μm	Chemokine speed half-concentration	0.005	Estimated
p_{max}	1/μm 1/min	Maximum proliferation pressure	5.99782	Macklin et al. (2012) and Hyun et al. (2013)
$\bar{p}_{max}$	dimensionless	Maximum proliferation “simple pressure”	219.79	Macklin et al. (2012) and Hyun et al. (2013)
R	μm	Radius of tumour slice	1269.7	**Figure S10**

R_{GBM}	μm	Radius of a glioblastoma cell	10.8	Oraiopoulou et al. (2017)
R_{CD4}	μm	Radius of a CD4+ T cell	3.6	Tasnim et al. (2018), Wang et al. (2014) and Du et al. (2017)
R_{CD8}	μm	Radius of a CD8+ T cell	3.6	Tasnim et al. (2018), Wang et al. (2014) and Du et al. (2017)
$R_{stromal}$	μm	Radius of a stromal cell	7.5	Freitas et al. (1999)
$r_{01,CD4}$	1/min	Transition from Ki67- to Ki67+	$7.9\times\ 10^{-5}$	**Figure S16**
$r_{01,CD8}$	1/min	Transition from Ki67- to Ki67+	$7.2\times\ 10^{-5}$	**Figure S16**
r_{10}	1/min	Division rate	0.00143	Kinjyo et al. (2015)
ρ^{*}_{virus}	amount/μm	Virus saturation concentration	268.51	Krol et al. (1999) and Dreher et al. (2006)
$\rho^{*}_{chemkokine}$	amount/μm	Chemokine saturation concentration	5	**Figure 3**E
ρ_{max}	virions/μm^3	Maximum binding density	0.0125	Estimated
$S_{chemokine}$	1/min	Secretion rate from CD4+ T cells	0.0417	**Figure 3**E
σ	dimensionless	Standard deviation for patch radius	0.4742μ	**Figure S12**
τ	min	Attached time CD8+ T cell to infected cell	50	Halle et al. (2016)
u_g	1/min 1/μm^3	Binding rate virus by glioblastoma cells	0.0020276	**Figure S15**
u_s	1/min 1/μm^3	Binding rate of virus by Stromal cells	0.01	Estimated
V_0	virions/μm^3	Initial concentration of virus (main text)	3.0248	**Figure S15**
$V_{N,GBM}$	μm^3	Total nuclear volume (glioblastoma cell)	740	Kouwenberg et al. (2018)
$V_{N,CD4}$	μm^3	Total nuclear volume (CD4+ T cell)	95.2	Rossi et al. (2019)

$V_{N,CD8}$	μm^3	Total nuclear volume (CD8+ T cell)	96.2	Rossi et al. (2019)
$V_{N,stromal}$	μm^3	Total nuclear volume (Stromal cell)	500	Ghaffarizadeh et al. (2018)
ξ	cells/μm^2	Density of tumour slice	0.9398	**Figure 3**C

Variables	Units	Description	Size	Variables
A_i	μm^2	Area of the ith band (where $i \in 1{:}N_b$)		*1x1*
A_{cell}	μm^2	Surface area of cell		*1x1*
b	dimensionless	Chemotaxis bias parameter ($0 < b < 1$)		*1x1*
$\boldsymbol{D}$	$\mu m^2/min$	Vector of diffusion coefficients		*2x1*
d_i	μm	Distance of cell from centre of the patch		*1x1*
d_{patch}	μm	Distance of patch centre from tumour slice centre		*1x1*
$\boldsymbol{d_{bias}}$	dimensionless	Bias direction		*1x1*
$F_{i,j}^{ccr}$	μm/min	Cell i-cell j repulsive force		*1x1*
f_{CN}	dimensionless	"target" cytoplasmic to nuclear volume ratio		*1x1*
$Ki67-$	cells	Number of non-proliferative cells		*1x1*
$Ki67+$	cells	Number of proliferative cells		*1x1*
κ	dimensionless	Area correction factor		*1x1*
$\boldsymbol{\lambda}$	1/min	Vector of decay rates		*2x1*
m_i	virions	Amount of intracellular virus in cell i		*1x1*
N_b	dimensionless	Number of bands		*1x1*
N_{GBM}	cells	Number of glioblastoma cells		*1x1*
$N_{stromal}$	cells	Number of stromal cells		*1x1*
n	Samples	Number of patients/tissue samples		*1x1*
ν	$\mu m/min$	Base cell speed		*1x1*
Ω	dimensionless	Relative ratio of virus binding of glioblastoma and stromal cells		*1x1*
Π(k)	dimensionless	Set of points that neighbour point k		*nx1*
$\bar{p}_i$		"simple pressure" on cell i		*1x1*
ψ	$\mu m/min$	Migration speed		*1x1*
$\boldsymbol{\phi}$	dimensionless	Random migration direction		*2x1*
R_i	μm	Radius of ith band (where $i \in 1{:}N_b$)		*1x1*
$R_{nucleus}$	μm	Radius of the nucleus		*1x1*
R_{cell}	μm	Radius of a cell		*1x1*
R_{patch}	μm	Radius of patch		*1x1*
$\boldsymbol{r}_k$	dimensionless	Position of the kth cell		*2x2*
$\boldsymbol{r}_{i,j}$	dimensionless	Vector between the ith and jth cell		*2x2*
$\boldsymbol{r}_{centre}$	dimensionless	Vector between cell and centre of the tumour slice		*2x2*
r_{sym}	dimensionless	Points symmetric to points within tumour slice domain		*2x1*
$\boldsymbol{\rho}$	amount/μm	Vector of concentrations		*2x1*
ρ_{virus}	amount/μm	Concentration of virus		*1x1*
$\rho_{chemokine}$	amount/μm	Concentration of chemokine		*1x1*
$\boldsymbol{\rho}^*$	amount/μm	Vector of saturation concentrations		*2x1*
$\boldsymbol{S}$	1/min	Vector of secretion rates		*2x1*
S_{virus}	1/min	Secretion rate for virus		*1x1*
$S_{chemokine}$	1/min	Secretion rate for chemokine		*1x1*
$\boldsymbol{s}$	μm	Distances between immune types		*1x1*
T	Min	Motility type persistance time		*1x1*

t	min	Time	*1x1*
θ_{cell}	radians	Angle of individual cell from centre of tumour slice	*1x1*
θ_{patch}	radians	Angle of patch from centre of tumour slice	*1x1*
$\boldsymbol{U}$	1/min	Vector of uptake (binding) rates	*2x1*
U_{virus}	1/min	Uptake (binding) rate of virus	*1x1*
$U_{chemokine}$	1/min	Uptake (binding) rate of chemokine	*1x1*
u	1/min $1/\mu m^3$	Base virion binding rate by cells	*1x1*
V_k	μm^3	Volume of kth cell	*1x1*
V_N	μm^3	Cell nuclear volume	*1x1*
V_S	μm^3	Solid biomass volume	*1x1*
V_C	μm^3	Total Cell cytoplasmic volume	*1x1*
V_{NS}^*	μm^3	"target" cell nuclear solid volume	*1x1*
V_{CS}	μm^3	Cell cytoplasmic solid volume	*1x1*
$\boldsymbol{v}_{mot}$	Dimensionless	Migration velocity vector	*2x1*